Structural Properties and Charge Distribution of the Sodium Uranium, Neptunium, and Plutonium Ternary Oxides

A Combined X-ray Diffraction and XANES Study

Smith, Anna L.; Martin, Philippe M.; Prieur, Damien; Scheinost, Andreas C.; Raison, Philippe E.; Cheetham, Anthony K.; Konings, Rudy J M

DOI
10.1021/acs.inorgchem.5b02476

Publication date
2016

Document Version
Final published version

Published in
Inorganic Chemistry: including bioinorganic chemistry

Inorganic Chemistry

Article

pubs.acs.org/IC

Structural Properties and Charge Distribution of the Sodium Uranium, Neptunium, and Plutonium Ternary Oxides: A Combined X-ray Diffraction and XANES Study

Anna L. Smith,[*,†,‡,§] Philippe Martin,[∥] Damien Prieur,[†] Andreas C. Scheinost,[⊥] Philippe E. Raison,[†] Anthony K. Cheetham,[‡] and Rudy J. M. Konings[*,†]

[†]European Commission, Joint Research Centre (JRC), Institute for Transuranium Elements (ITU), P.O. Box 2340, D-76125 Karlsruhe, Germany

[‡]Department of Materials Science and Metallurgy, University of Cambridge, 27 Charles Babbage Road, Cambridge CB3 0FS, United Kingdom

[∥]CEA, DEN, DEC, CEN Cadarache, 13108 St. Paul Lez Durance, France

[⊥]Helmholtz Zentrum Dresden Rossendorf (HZDR), Institute of Resource Ecology, P.O. Box 10119, 01314 Dresden, Germany

Supporting Information

ABSTRACT: The charge distributions in α-Na_2UO_4, Na_3NpO_4, α-Na_2NpO_4, Na_4NpO_5, Na_5NpO_6, Na_2PuO_3, Na_4PuO_5, and Na_5PuO_6 are investigated in this work using X-ray absorption near-edge structure (XANES) spectroscopy at the U-L_3, Np-L_3, and Pu-L_3 edges. In addition, a Rietveld refinement of monoclinic Na_2PuO_3, in space group $C2/c$, is reported for the first time, and the existence of the isostructural Na_2NpO_3 phase is revealed. In contrast to measurements in solution, the number of published XANES data for neptunium and plutonium solid phases with a valence state higher than IV is very limited. The present results cover a wide range of oxidation states, namely, IV to VII, and can serve as reference for future investigations. The sodium actinide series show a variety of local coordination geometries, and correlations between the shape of the XANES spectra and the local structural environments are discussed herein.

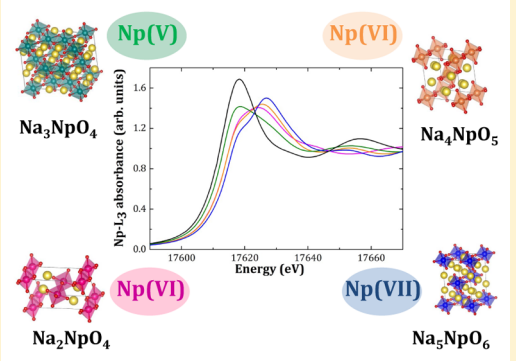

INTRODUCTION

Considerable interest in the structural, thermomechanical, and thermodynamic properties of the phases forming in the Na−(U,Np,Pu)−O systems has existed since the 1960s because of their technological importance for sodium-cooled fast reactors (SFRs).[1,2] Among the six designs retained by the Generation IV International Forum (GIF), the SFR is the most advanced concept and probably the first one to move to a demonstration phase and commercial deployment.[1] Sodium is particularly interesting as a metallic coolant as it shows a high boiling point (1156 K), a high heat capacity, and a good thermal conductivity.[1,2] From safety perspectives, it is essential, however, to gain a thorough knowledge of the products of interaction between the sodium metallic coolant and the nuclear fuel, as the two might come into contact in the accidental event of a breach of the stainless steel cladding. $(U,Pu)O_2$ mixed oxide (MOX) fuels are currently the preferred choice for SFRs as substantial experience has already been gained in terms of fabrication, reactor operation, reprocessing, and risk assessment. In addition, the incorporation into the fuel of the minor actinide elements (Np, Am, Cm) generated during irradiation in the current fleet of nuclear reactors is also envisaged to reduce their radiotoxicity by transmuting them into radioactive elements with shorter half-lives.[3,4]

The chemistry of the sodium and $(U,Pu,Np,Am,Cm)O_2$ nuclear fuel interaction is complex. The potential reaction products are numerous: Na_2NpO_3, Na_2PuO_3, $NaUO_3$, Na_3AnO_4, Na_2UO_4, Na_2NpO_4, Na_4AnO_5, $Na_2An_2O_7$, Na_5NpO_6, and Na_5PuO_6 (An = U, Np, Pu), but not all well characterized.[5−9] Past studies carried out in the 1980s have shown that the reaction between sodium and $(U,Pu)O_2$ fuel leads in the temperature range of the fuel during operation, close to the pellet rim (around 893−923 K[10]), to the formation of sodium urano−plutonates $Na_3(U_{1-x},Pu_x)O_4$[11−13] of lower density and lower thermal conductivity relative to the mixed oxide fuel.[14−16] Such a situation can induce further cladding failure, restrain the flow of coolant within a subassembly of fuel pins, or result in a contamination of the primary coolant with the fuel elements comprising plutonium, minor actinides, and fission products.[14−16] For a thorough safety assessment of the interaction, a sound knowledge of the sodium actinide oxide phases is hence required.

Received: October 26, 2015
Published: February 2, 2016

DOI: 10.1021/acs.inorgchem.5b02476
Inorg. Chem. 2016, 55, 1569−1579

Table 1. Summary of the Synthesis Conditions Used in This Work to Prepare the Sodium Uranates, Neptunates, and Plutonates

material	reactants	container	gas	T (K)	color	impurity mass fraction
sodium uranates						
$NaUO_3$	provided by NRG (Petten)				orange	none
Na_4UO_5	provided by NRG (Petten)				orange	none
α-Na_2UO_4	$(UO_2{:}Na_2CO_3) = (1{:}1)$	alumina	O_2	1103 (48 h)	orange	(0.2% Na_4UO_5)
sodium neptunates						
Na_2NpO_3	$(NpO_2{:}Na_2O_{1.14(1)}) = (1{:}2.2)$	stainless steel	Ar	1073 (24 h)	black	(1.8% NpO_2)
α-Na_3NpO_4	$(NpO_2{:}Na_2O_{1.14(1)}) = (1{:}2.4)$	stainless steel	Ar	1123 (24 h)	red/brown	none
α-Na_2NpO_4	$(NpO_2{:}Na_2O_{1.14(1)}) = (1{:}2)$	alumina	O_2	943 (48 h)	forest green	none
Na_4NpO_5	$(NpO_2{:}Na_2CO_3) = (1{:}2)$	alumina	O_2	1093 (70 h)	lime green	(0.5% Na_2NpO_4)
Na_5NpO_6	$(NpO_2{:}Na_2CO_3) = (1{:}3)$	alumina	O_2	1093 (60 h)	forest green	none
sodium plutonates						
Na_2PuO_3	$(PuO_2{:}Na_2CO_3) = (1{:}2)$	alumina	Ar	1123 (24 h)	black	(2.8% PuO_2)
Na_4PuO_5	$(PuO_2{:}Na_2CO_3) = (1{:}1.9)$	alumina	O_2	1093 (34h)	red	(4.5% Na_5PuO_6 + 1.7% PuO_2)
Na_5PuO_6	$(PuO_2{:}Na_2CO_3) = (1{:}3)$	alumina	O_2	1093 (34h)	black	none

Temperature and oxygen potential within the nuclear fuel and sodium coolant are the two fundamental parameters that control the chemistry of the interaction. To assess the margin to the safe operation of SFRs, the valence state of the actinide cation in the various sodium actinide oxide phases must be known as the latter determines the oxygen potential threshold required for the formation of the ternary compounds.[17−19] Thermodynamic calculations have in particular shown that the threshold for pentavalent $Na_3(U_{1-x},Pu_x)O_4$ phases was reached with the in-pile conditions.[17] X-ray diffraction allows one to identify the nature of the phases formed and characterize their structures. It cannot give a definite signature of the oxidation state of the actinide cation, however. X-ray absorption near edge structure (XANES) spectroscopy can provide information on the charge distribution, which is key for the safety assessment of the SFR.

In the present work, XANES spectroscopy measurements of α-Na_2UO_4, Na_3NpO_4, α-Na_2NpO_4, Na_4NpO_5, Na_5NpO_6, Na_2PuO_3, Na_4PuO_5, and Na_5PuO_6 are presented at the U-L_3, Np-L_3, and Pu-L_3 edges, covering a wide range of valence states, namely, from IV to VII. We also report for the first time the structural refinement of monoclinic Na_2PuO_3, and the existence of Na_2NpO_3 is revealed. By contrast with neptunium and plutonium phases in solution, there is a real lack in the literature of Np and Pu solid state XANES data with an oxidation state higher than IV.[20] Our work can serve as reference for future investigations, to determine either the valence state of an unknown composition or the ratio between different valence states in a mixed valence state compound.

MATERIALS AND METHODS

Solid State Synthesis. The $NaUO_3$ and Na_4UO_5 materials were kindly provided by NRG (Nuclear Research and Consultancy Group, Petten, Netherlands). The remaining phases were prepared by grinding together accurately weighted samples of depleted uranium dioxide ($^{238}UO_2$ from JRC-ITU stocks), neptunium dioxide ($^{237}NpO_2$ from ORNL, Oak Ridge National Laboratory), and plutonium dioxide (PuO_2 from JRC-ITU stocks with the isotopic composition 0.05% ^{238}Pu, 86.10% ^{239}Pu, 13.39% ^{240}Pu, 0.32% ^{241}Pu, 0.14% ^{242}Pu, 1.45% ^{241}Am (thermal ionization mass spectrometry and high resolution gamma spectroscopy measurements) with sodium oxide (Na_2O 82.1% + Na_2O_2 14.8%, ABCR GmbH & Co, i.e., $Na_2O_{1.14(1)}$) or sodium carbonate (Na_2CO_3 99.95%, Sigma).

^{238}U is an α emitter with a very long half-life (4.47 billion years),[21] making it only weakly radioactive. ^{237}Np decays to ^{233}Pa by α emission with a half-life of 2.14 million years. The ^{233}Pa daughter product is a β^- emitter with a very short half-life (27 days) and significant γ dose rate [1.335×10^{-4} (mSv/h)/MBq].[21] The plutonium batch used in this work showed an appreciable amount of highly radioactive ^{241}Am (half-life of 432.2 years) and associated γ dose rate [8.479×10^{-5} (mSv/h)/MBq].[21] The handling of those materials requiring considerable safety precautions was therefore done with limited quantities in alpha-glove boxes.

Sodium oxide was carefully stored in the dry atmosphere of an argon-filled glovebox because of its hygroscopic nature. The synthesized materials were moreover handled exclusively in nitrogen-filled or argon-filled alpha-glove boxes and stored under vacuum as some of the phases were found to be hygroscopic and to decompose over several months to $Na_2Np_2O_7$ by reaction with atmospheric water. The integrity of the products was also verified shortly before the XANES experiments using X-ray diffraction.

The mixtures were placed into an alumina crucible or a tightly closed stainless steel container and heated under argon or oxygen flow in a tubular furnace to stabilize the actinide cation in its oxidation states IV/V or VI/VII, respectively. Because of the significant γ dose rates of the neptunium and plutonium materials, the syntheses were performed with no more than 60 mg of neptunium dioxide or plutonium dioxide. Successive regrinding and 12 h heating steps were used to improve the crystallinity. A summary of the synthesis conditions for each composition is provided in Table 1.

X-ray Powder Diffraction. The samples were characterized at room temperature by X-ray diffraction using a Bruker D8 X-ray diffractometer mounted in the Bragg−Brentano configuration with a curved Ge monochromator (111) and a ceramic copper tube (40 kV, 40 mA) and equipped with a LinxEye position sensitive detector. The data were collected by step scanning in the angle range $10° \leq 2\theta \leq 120°$ with an integration time of about 8 h, a count step of 0.02° (2θ), and a dwell of 5 s/step. Structural analysis and quantification of eventual impurities were performed by the Rietveld method with the Fullprof2k suite.[22] The material purity was found to be better than 97.2% (except for the Na_4PuO_5 material pure at 93.8%) (see Table 1). The error introduced by those impurities on the position of the inflection points and white lines is within the uncertainty range of the XANES method at the An-L_3 edges (An = U, Np, Pu).

X-ray Absorption Near Edge Structure (XANES) Spectroscopy. XANES measurements were performed at the Rossendorf BeamLine (ROBL)[23] of the European Synchrotron Radiation Facility (ESRF, Grenoble, France). Small amounts (5−10 mg) of powdered sample were mixed with boron nitride (BN) in an argon-filled alpha-glovebox and pressed into pellets for the measurements. The storage ring operating conditions were 6.0 GeV and 170−200 mA. A double-crystal monochromator mounted with a Si(111) crystal coupled to collimating and focusing Rh-coated mirrors was used.

XANES spectra were collected at room temperature in transmission mode at the U-L_3, Np-L_3, and Pu-L_3 edges. A step size of 0.5 eV was used in the edge region. The energy E_0 of the edge absorption

DOI: 10.1021/acs.inorgchem.5b02476
Inorg. Chem. 2016, 55, 1569−1579

Table 2. Summary of the Structural Parameters at Room Temperature of the Sodium Uranates, Neptunates, and Plutonates, γ-UO_3, and $UO_2(NO_3)_2{\cdot}6H_2O$

compound	$NaUO_3$	Na_4UO_5	α-Na_2UO_4	γ-UO_3	$UO_2(NO_3)_2{\cdot}6H_2O$
U valence	V	VI	VI	VI	VI
symmetry	orthorhombic	tetragonal	orthorhombic	tetragonal	orthorhombic
Z	4	2	2	16	4
space group	*Pbnm* (62)	*I*4/*m* (87)	*Pbam* (55)	$I4_1/amd$ (141)	$Cmc2_1$ (36)
a (Å)	5.7739(2)	7.5172(1)	9.7623(3)	6.9013(5)	13.197(3)
b (Å)	5.9051(2)	7.5172(1)	5.7287(2)	6.9013(5)	8.035(3)
c (Å)	8.2784(2)	4.6325(2)	3.4956(1)	19.9754(18)	11.467(3)
β (deg)	90	90	90	90	90
vol. (Å^3)	282.26(1)	261.78(1)	195.496(11)	951.39(1)	1215.9(1)
ref	25	29	28	31	32

compound	Na_2NpO_3	Na_3NpO_4	α-Na_2NpO_4	Na_4NpO_5	Na_5NpO_6
Np valence	IV	V	VI	VI	VII
symmetry	monoclinic	orthorhombic	orthorhombic	tetragonal	monoclinic
Z	8	8	2	2	2
space group	*C*2/*c* (69)	*Fmmm* (69)	*Pbam* (55)	*I*4/*m* (87)	*C*2/*m* (12)
a (Å)	5.999(3)	13.353(3)	9.715(3)	7.535(3)	5.829(3)
b (Å)	10.371(3)	9.629(3)	5.732(3)	7.535(3)	9.996(3)
c (Å)	11.796(3)	6.673(3)	3.459(3)	4.616(3)	5.757(3)
β (deg)	109.97(1)	90	90	90	110.73(1)
vol. (Å^3)	689.77(1)	857.99(1)	192.59(1)	262.08(1)	313.78(1)
ref	this work	30	6	30	30

compound	Na_2PuO_3	Na_3PuO_4	Na_4PuO_5	Na_5PuO_6
Pu valence	IV	V	VI	VII
symmetry	monoclinic	orthorhombic	tetragonal	monoclinic
Z	8	8	2	2
space group	*C*2/*c* (69)	*Fmmm* (69)	*I*4/*m* (87)	*C*2/*m* (12)
a (Å)	5.965(3)	13.302(2)	7.519(2)	5.823(3)
b (Å)	10.313(3)	9.634(2)	7.519(2)	9.985(3)
c (Å)	11.772(3)	6.651(2)	4.619(1)	5.752(3)
β (deg)	109.97(1)	90	90	110.79(1)
vol. (Å^3)	680.56(1)	852.34(1)	261.14(1)	312.65(1)
ref	this work	30	9	19

threshold position was taken at the first inflection point of the spectrum by using the first node of the second derivative. The position of the white-line maximum was selected from the first node of the first derivative. Several acquisitions were performed on the same sample and summed up to improve the signal-to-noise ratio. Before averaging the scans, each spectrum was aligned using the XANES spectrum of a metallic reference foil located between the second and the third ionization chambers and measured at the same time as the sample. Yttrium (17 038 eV) was used at the U-L_3 and Np-L_3 edges, while zirconium (17 998 eV) was used at the Pu-L_3 edge. The ATHENA software (Version 0.9.20)[24] was used to remove the background and to normalize the spectra.

RESULTS AND DISCUSSION

Structural Properties of the Sodium Actinide Ternary Oxides. The structural parameters of the sodium actinide ternary oxides investigated herein are summarized in Table 2. Tetravalent UO_2, NpO_2, and PuO_2, which are not mentioned in the table, are cubic, in space group $Fm\bar{3}m$. Pentavalent $NaUO_3$ has a perovskite structure, in space group *Pbnm*.[25] $NaNpO_3$ and $NaPuO_3$ were never reported in the literature and can probably not be synthesized as stable phases. Pentavalent Na_3NpO_4 and Na_3PuO_4 are orthorhombic, in space group *Fmmm*.[26] The case of trisodium uranate Na_3UO_4 is particularly complex[27] and not discussed further in the present work. We refer the reader to refs 26 and 27 for more detail on this particular composition. Hexavalent α-Na_2UO_4 and α-Na_2NpO_4 are isostructural and show orthorhombic symmetry, in space group *Pbam*.[6,28] Na_2PuO_4 could not be synthesized as a stable phase, however. The Na_4AnO_5 (An = U, Np, Pu) composition is common to all three systems with a tetragonal structure, in space group *I*4/*m*.[9,29,30] Heptavalent Na_5NpO_6 and Na_5PuO_6 are both monoclinic, in space group *C*2/*m*.[19,30] All of these ternary oxide phases show 6-fold-coordinated actinide cations as described in detail in the following sections. Moreover, the mean U−O, Np−O, and Pu−O distances in the AnO_6 octahedra decrease when the valence state of the actinide cation increases, which is expected from the size of the respective ionic radii, as reported in ref 26.

Structural Characterization of Na_2PuO_3 and Na_2NpO_3. The case of Na_2PuO_3 requires particular attention, as the assignment of its crystal structure is not straightforward. Bykov et al. suggested two possible indexations: a rhombohedral cell in space group $R\bar{3}m$ and a monoclinic cell in space group *C*2/*c* based on the model of Na_2CeO_3.[33,34] None of the descriptions were completely satisfactory, however, and could reproduce all the observed reflections. In addition, the authors reported slightly different X-ray diffraction patterns depending on the synthesis conditions. In fact, a similar situation was already described for Na_2RuO_3,[35] which was refined using a superposition of two phases with rhombohedral ($R\bar{3}m$) and monoclinic (*C*2/*c*) symmetries, corresponding to a disordered and ordered state, respectively. Bykov et al. reported refined

DOI: 10.1021/acs.inorgchem.5b02476
Inorg. Chem. 2016, 55, 1569−1579

atomic positions based on the rhombohedral model in space group $R\bar{3}m$ (the corresponding refinement excluding some of the experimentally observed reflections between 16.5° and 28.0°). However, the authors also suggested that a description using a partial ordering model was needed, with a degree of ordering varying depending on the synthesis conditions. The structural properties of Na_2PuO_3 were therefore reinvestigated in this work in an attempt to settle the unresolved issues raised in the paper of Bykov et al.[9] In addition, the possible existence of Na_2NpO_3 was examined. Although there is no report in the literature of the existence of such a phase for neptunium, one could expect Na_2NpO_3 to be stable as the ionic radius of 6-fold-coordinated Np^{4+} (0.87 Å) is the same as for Ce^{4+} (0.87 Å) and slightly larger than for Pu^{4+} (0.86 Å).[36]

Na_2PuO_3 was prepared using a different synthesis route compared to the work of Bykov et al.,[9] who heated a mixture of plutonium dioxide and sodium oxide under argon either in an alumina boat or in a tightly closed stainless steel container. In this work, plutonium dioxide and sodium carbonate were mixed in a PuO_2:Na_2CO_3 = 1:2 ratio and heated in an alumina boat under argon flow at 1123 K for 24 h (Table 1), leading to the formation of Na_2PuO_3 together with unreacted PuO_2 (2.8%). Na_2NpO_3 was synthesized for the first time by mixing neptunium dioxide and sodium oxide in a NpO_2:$Na_2O_{1.14(1)}$ = 1:2.2 ratio, and heating the mixture at 1073 K for 24 h in a stainless steel container tightly closed under the purified Ar atmosphere of the glovebox (Table 1). The synthesis route using sodium carbonate was also attempted but led to the formation of pentavalent Na_3NpO_4,[26] due to the less reducing atmospheric conditions.

The monoclinic model of Na_2CeO_3, in space group $C2/c$, was selected for the refinement of the X-ray diffraction data of Na_2PuO_3 in favor of the rhombohedral one (space group $R\bar{3}m$), as the latter structure failed to reproduce the low-intensity reflections observed at 2θ values 17.2°, 17.3°, 18.0°, 20.2°, 23.6°, and 27.7° (Figure 1). The refinement yielded cell parameters as a = 5.965(3) Å, b = 10.313(3) Å, c = 11.772(3) Å, and β = 109.97(1)°. The refined atomic positions and bond lengths are listed in Tables 3 and 4. The corresponding cell volume, i.e., 680.56(1) Å^3, is sligthly smaller than for the isostructural cerium compound, which is consistent with the ionic radii of Pu^{4+} and Ce^{4+}.[36]

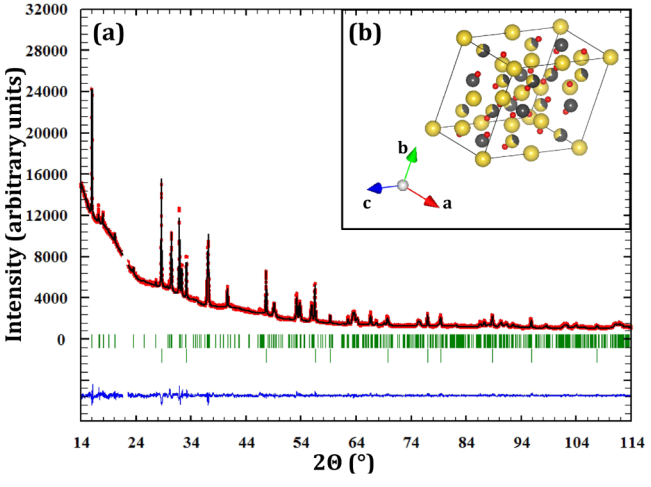

Figure 1. (a) Comparison between the observed (Y_{obs}, in red) and calculated (Y_{calc}, in black) X-ray diffraction patterns of Na_2PuO_3. $Y_{obs} - Y_{calc}$, in blue, is the difference between the experimental and calculated intensities. Bragg reflections are marked in green. (Top) Na_2PuO_3. (Bottom) PuO_2. Measurement at λ = Cu Kα1. The broad featureless response at low 2θ angles and excluded region (corresponding to a broad reflection) are coming from the glue used for encapsulation of the plutonium sample. (b) Crystal structure of Na_2PuO_3 (Pu atoms in gray, Na atoms in yellow, O atoms in red).

Our results provide for the first time a refinement of the Na_2PuO_3 structure based on the ordered monoclinic model of Na_2CeO_3. However, complementary studies involving "quenching" experiments are needed to clarify the relationships between the ordered (monoclinic) and the disordered (rhombohedral) structures of Na_2PuO_3 obtained using different synthesis routes, as illustrated by the present results and those of Bykov et al.[9]

The X-ray diffraction pattern obtained for Na_2NpO_3 showed again small reflections at 2θ values of 17.1°, 17.2°, 17.9°, 18.2°, 20.0°, 23.4°, and 27.5°, suggesting the monoclinic model should also be selected. The crystallinity of the sample was unfortunately not good enough to perform a Rietveld refinement. A Le Bail fit[37] yielded cell parameters as a = 5.999(3) Å, b = 10.371(3) Å, c = 11.796(3) Å, and β = 109.97(1)°, which corresponds to a cell volume of 689.77(1) Å^3. These data are compared in Figure 2a, 2b, and 2c to those reported for Na_2PdO_3,[38] Na_2RuO_3,[35] Na_2PtO_3,[39] Na_2TbO_3,[34] Na_2PrO_3,[34] and Na_2CeO_3,[33] which all have the same monoclinic structure, as was done in the work of Bykov et al.[9] The unit cell parameters and volume of Na_2NpO_3 are in very good agreement with the general trend along this series. Interestingly, the isostructural uranium compound was never reported. It is probable that Na_2UO_3 cannot form as a stable phase due to the rather large ionic radius of U^{4+} (0.89 Å) compared to Np^{4+} (0.87 Å), Ce^{4+} (0.87 Å), and Pu^{4+} (0.86 Å).[36]

XANES Spectroscopy of Sodium Uranates. XANES spectra of $NaUO_3$ and Na_4UO_5 collected at the U-L_3 edge were recently published,[5] together with the energy positions of the inflection points and white lines due to (2p → 6d) transitions.[5] Those results have confirmed the uranium valence states, namely, V and VI for $NaUO_3$ and Na_4UO_5, respectively. In the present work, we report the XANES spectrum for α-Na_2UO_4 (Figure 3) to complete this series of measurements. The inflection point and white line (WL) positions of α-Na_2UO_4, listed in Table 5, are perfectly aligned with those of $U^{(VI)}O_3$, $Na_4U^{(VI)}O_5$, and $U^{(VI)}O_2(NO_3)_2{\cdot}6H_2O$. These results are hence consistent with uranium being exclusively in the oxidation state VI in α-Na_2UO_4 and therefore having a $[Rn]5f^0$ electronic configuration. With increasing formal valence state, the values of the inflection points are shifted to higher energy as a consequence of the decreasing Coulomb energies in the final state between the 5f and excited 6d electrons and the $2p_{3/2}$ core hole.[40−42]

It can be noted in Figure 3 and Table 5 that the reference $U^{(IV)}O_2$ compound shows a single WL peak, while the sodium uranates of higher valence state show double-peaked WLs. The low-energy shoulder observed in $NaU^{(V)}O_3$ is an intrinsic feature of the uranium unoccupied 6d electronic states of the U(V).[43] The double-peak WL feature in $U^{(VI)}O_3$ was interpreted in terms of core-ionized final states with different 5f occupancies in reported work.[40,41] Bertram and co-workers performed in the 1980s a high-pressure XANES experiment on UO_3 at the U-L_3 edge and found that the distance between the two WLs was reduced with pressure as well as the relative intensity of peak A compared to peak B (see Figure 3). The application of pressure induces an increased 5f covalency. Peak

DOI: 10.1021/acs.inorgchem.5b02476
Inorg. Chem. 2016, 55, 1569−1579

Table 3. Refined Atomic Positions in Na_2PuO_3[a]

atom	ox. state	Wyckoff	x	y	z	B_0 (Å^2)	occupancy
Pu1	+4	4e	0	0.835(5)	0.25	0.27(2)	0.35
Na1	+1	4e	0	0.835(5)	0.25	0.27(2)	0.65
Pu2	+4	4e	0	0.169(3)	0.25	0.27(2)	0.65
Na2	+1	4e	0	0.169(3)	0.25	0.27(2)	0.35
Pu3	+4	4e	0	0.498(2)	0.25	0.27(2)	1
Na3	+1	4a	0	0	0	0.27(2)	1
Na4	+1	8f	0.036(4)	0.340(4)	0.013(2)	0.27(2)	1
O1	−2	8f	0.247(8)	0.495(9)	0.142(4)	1.00(8)	1
O2	−2	8f	0.249(9)	0.141(5)	0.175(3)	1.00(8)	1
O3	−2	8f	0.271(9)	0.839(9)	0.132(4)	1.00(8)	1

[a] R_{wp} = 18.60, R_{exp} = 11.92, χ^2 = 2.44.

Table 4. Selected Bond Lengths, R, for Na_2PuO_3 Derived from the X-ray Diffraction Refinement[a]

bond	N	R (Å)	bond	N	R (Å)
Pu(1)−O(1)	2	2.30(9)	Na(3)−O(1)	2	2.61(5)
Pu(1)−O(2)	2	2.47(6)	Na(3)−O(1)	2	2.54(4)
Pu(1)−O(3)	2	2.47(6)	Na(3)−O(2)	2	2.46(7)
Pu(2)−O(1)	2	2.41(9)	Na(4)−O(1)	1	2.27(9)
Pu(2)−O(2)	2	1.99(5)	Na(4)−O(1)	1	2.64(8)
Pu(2)−O(3)	2	2.36(8)	Na(4)−O(2)	1	2.79(5)
Pu(3)−O(1)	2	2.25(5)	Na(4)−O(2)	1	2.92(6)
Pu(3)−O(2)	2	2.07(5)	Na(4)−O(3)	1	2.44(6)
Pu(3)−O(3)	2	2.28(7)	Na(4)−O(3)	1	2.75(8)

[a] Standard deviations are given in parentheses. N is the number of atoms in each coordination shell.

A, whose position is not influenced by the application of pressure, was thereafter mainly attributed to a $5f^0$ final-state configuration. Peak B, whose intensity is increased and whose position is shifted to higher energy, was assigned to a $5f^2/5f^1$ covalently mixed state.

The shape of the XANES spectra is often related in the literature to the local coordination environment around the actinide cation. In particular, the shoulder and reduced peak amplitude observed in U(VI) compounds about 15 eV above the U edge (γ-UO_3 for instance which shows two U−O distances at 1.887(5) Å in the axial direction and four U−O distances at 2.230(3) Å in the equatorial plane of the UO_6 octahedra) is a feature attributed to the linear $[O{=}U{=}O]^{2+}$ group of the uranyl compounds, which causes localized multiple-scattering resonance.[42] Among the sodium uranates measured herein, only α-Na_2UO_4 shows the uranyl type of coordination, with two short bonds at 1.903(2) Å along the axial direction and four longer bonds at 2.013(4) Å (Table 6) in the equatorial plane of the UO_6 octahedra. However, the presence of a secondary shoulder is not obvious in this case. The spectrum shows a rather unexpected shape: the two WLs seem to merge and are less resolved, while the main WL is found about 4 eV above the WL of UO_3. More surprisingly, Na_4UO_5 which has the "reverse" uranyl type of configuration, with two long axial bonds at 2.3163(1) Å and four short equatorial bonds at 2.013(1) Å, shows a spectrum very similar to that of γ-UO_3. As for $UO_2(NO_3)_2{\cdot}6H_2O$, finally, the inflection point and main white line are well aligned with those of γ-UO_3 and Na_4UO_5, but the secondary shoulder is found at much higher energy (about 20 eV above E_0). In this case, the uranyl group with U−O distances at 1.770(7) and 1.749(7) Å, respectively, is surrounded in the equatorial plane by four oxygen atoms belonging to the bidentate nitrate groups and two water oxygens. The uranyl angle in the axial direction is nearly linear (179.1°). The present results therefore suggest that the XANES features usually associated with multiple scattering of the U(VI) uranyl could have a different origin, possibly core ionized final states with different 5f occupancies, as suggested in the work of Bertram and co-workers.[40,41]

XANES Spectroscopy of Sodium Neptunates. The XANES spectra of the sodium neptunate phases collected at the Np-L_3 edge are shown in Figure 4 together with the spectrum of the $Np^{(IV)}O_2$ reference material. The energy positions of the inflection points and of the white lines are provided in Table 5.

The valence states of the sodium neptunates were recently revealed in our research group by ^{237}Np Mössbauer spectroscopy from the values of their respective isomer shifts.[26,30,45] This technique gives direct insight into the hyperfine interactions between the nucleus and its surrounding electrons.[46] In particular, it yields information on the electronic, magnetic, and local structural properties of the materials investigated through the measurement of the electric monopole (Coulomb) interaction (or isomer shift), magnetic coupling, and electric quadrupole coupling constant, respectively. The isomer shift yields a univocal signature of the Np valence state. The values obtained in our research group, shown in the correlation diagram in Figure 5, correspond to Np(V) for Na_3NpO_4,[26] Np(VI) for α-Na_2NpO_4[45] and Na_4NpO_5,[30] and Np(VII) for Na_5NpO_6.[30]

The XANES series for neptunium is particularly interesting as the results can be compared with those obtained by ^{237}Np Mössbauer spectroscopy. Figure 6 shows a linear variation of the absorption edge threshold E_0 determined by XANES versus the Mössbauer isomer shift values. The isomer shift results from the Coulomb interaction between the nuclear charge and the charge of the surrounding electrons. It is proportional to the difference in electronic charge density ($\Delta\rho_e$) between the source material and the absorber at the nuclear origin: $\delta_{IS} = \alpha{\cdot}\Delta\rho_e(0)$ (α being a calibration constant). $\Delta\rho_e$ mainly originates from $s_{1/2}$ and $p_{1/2}$ shells. However, the f shells also have an influence on this number as they produce a shielding effect on the charge density of the inner shells. A removal of 5f electrons, corresponding to reduced shielding, leads to an increase of $\rho_e(0)$. As for the inflection point, it is shifted to higher energy with increasing formal valence state as a consequence of the decreasing Coulomb energies in the final state between the 5f and excited 6d electrons and the $2p_{3/2}$ core hole[40−42] as stated before. It is hence not surprising to find a correlation between those two quantities. In the 1980s, Bertram and co-workers already reported a similar relationship between

DOI: 10.1021/acs.inorgchem.5b02476
Inorg. Chem. 2016, 55, 1569−1579

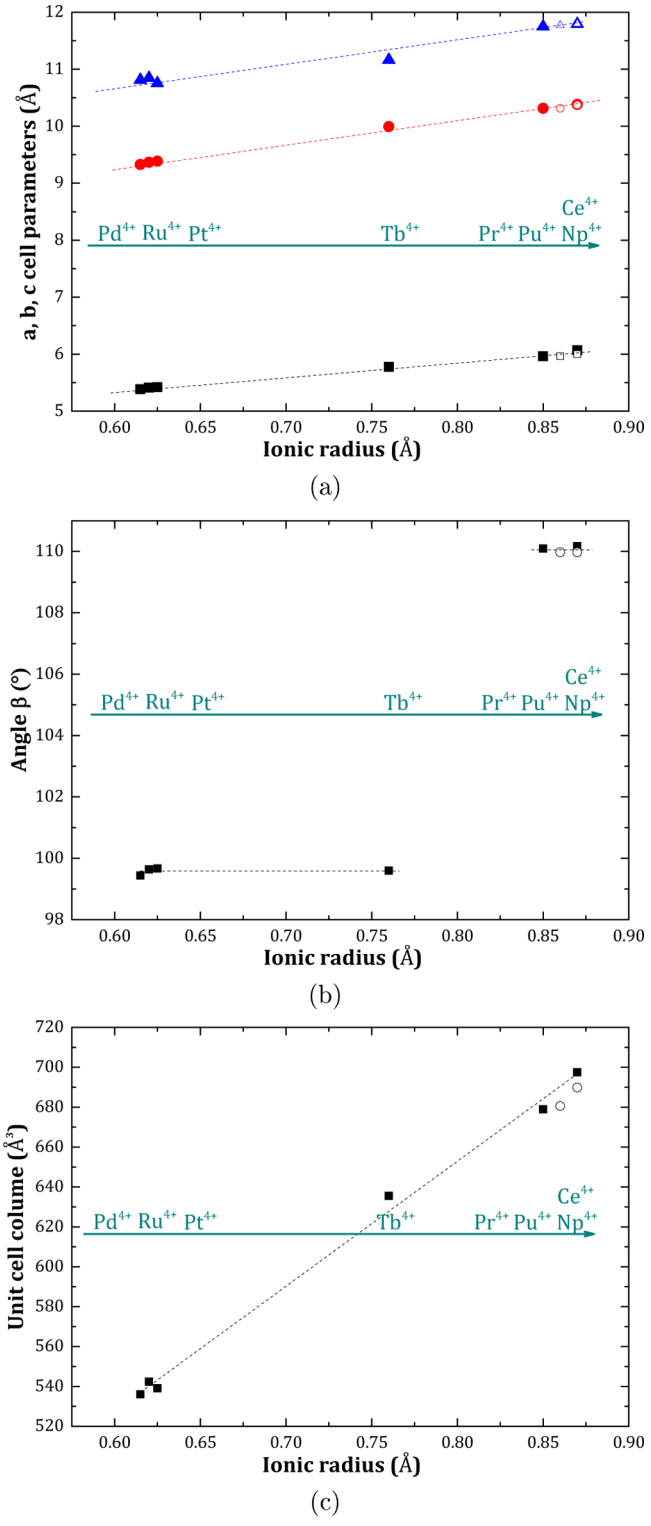

Figure 2. (a and b) Evolution of the unit cell parameters and (c) unit cell volume along the Na_2MO_3 series (M = Pd, Ru, Pt, Tb, Pr, Ce) (■) and Na_2AnO_3 series (An = Np,Pu) (○) as a function of the ionic radius of the M^{4+} (respectively, An^{4+}) cation.[36]

the isomer shift and the weighted mean position of the white line peaks for neptunium nonmetallic compounds.[40,41]

In a similar way to the uranium series, the reference $Np^{(IV)}O_2$ compound exhibits a single WL peak, while the measured sodium neptunates, which all have a higher Np valence state, exhibit double-peaked WLs. The same observation was already

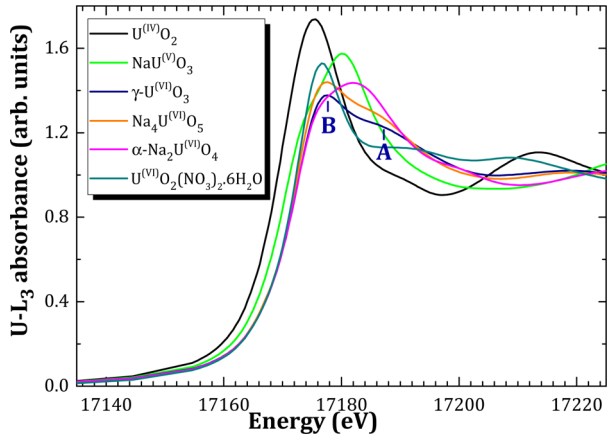

Figure 3. Normalized XANES spectra of $UO_2(NO_3)_2{\cdot}6H_2O$, α-Na_2UO_4 (present work), $NaUO_3$, Na_4UO_5, together with UO_2 and UO_3 reference materials.[5]

Table 5. Energies of the Inflection Points and White Lines of the U-L_3, Np-L_3, and Pu-L_3 XANES Spectra[a]

compound	inflection point (eV)	white line (eV)		ref
uranium				
UO_2	17 169.9(5)	17 175.5(5)		5
$NaUO_3$	17 170.4(5)	*17 175.1(5)*	17 180.1(5)	5
γ-UO_3	17 172.8(5)	17 177.7(5)	*17 186.7(5)*	5
Na_4UO_5	17 172.7(5)	17 177.6(5)	*17 186.5(5)*	5
α-Na_2UO_4	17 172.5(5)	17 181.9(5)		b
$UO_2(NO_3)_2{\cdot}6H_2O$	17 172.8(5)	17 176.7(5)	*17 192.7(5)*	b
neptunium				
NpO_2	17 612.1(5)	17 618.3(5)		b
Na_3NpO_4	17 613.4(5)	17 618.5(5)		b
α-Na_2NpO_4	17 614.2(5)	17 624.3(5)		b
Na_4NpO_5	17 614.1(5)	*17 618.8(5)*	17 625.6(5)	b
Na_5NpO_6	17 615.1(5)	*17 619.0(5)*	17 626.9(5)	b
plutonium				
PuO_2	18 062.4(5)	18 067.6(5)		b
Na_2PuO_3	18 062.1(5)	18 067.7(5)		b
Na_4PuO_5	18 062.9(5)	*18 067.3(5)*	18 073.3(5)	b
Na_5PuO_6	18 063.5(5)	18 069.0(5)	*18 082.3(5)*	b

[a]The secondary white line, if present, is listed in italics. [b]This work.

made in the literature for the $Na_4(Np^{(V)}O_2)_2C_{12}O_{12}{\cdot}8H_2O$, $Na_2Np^{(VI)}{}_2O_7$, $Ba_2CoNp^{(VI)}O_6$, and $CsNp^{(VII)}O_4$ compounds when compared to NpI_3 and NpO_2[40,41] and was interpreted in terms of core-ionized final states with different 5f occupancies. Unfortunately, the latter authors did not report the values of the inflection points and white lines for their data, so that a direct comparison with the present measurement is not possible.

In contrast to the cubic symmetry of the neptunium cation in $Np^{(IV)}O_2$, the sodium neptunates show distorted local structures in 6-fold coordination (Table 7). $Na_3Np^{(V)}O_4$ and α-$Na_2Np^{(VI)}O_4$ both have a neptunyl type of coordination, with two close oxygen neighbors in the axial direction at 2.066(6) Å for $(NpO_2)^+$ and 1.762(5) Å for $(NpO_2)^{2+}$, respectively (Table 8). $Na_3Np^{(V)}O_4$ shows the characteristic secondary shoulder and reduced peak amplitude expected for the neptunyl but not α-$Na_2Np^{(VI)}O_4$. In fact, the spectrum of α-Na_2NpO_4 resembles

DOI: 10.1021/acs.inorgchem.5b02476
Inorg. Chem. 2016, 55, 1569−1579

Table 6. Local Geometry, Bond Lengths, and Bond Angles around the Uranium Cation in UO_2, $NaUO_3$, α-Na_2UO_4, Na_4UO_5, γ-UO_3, and $UO_2(NO_3)_2{\cdot}6H_2O$

bond length or angle (Å or deg)	UO_2[44]	$NaUO_3$[25]	α-Na_2UO_4[28]	Na_4UO_5[29]
U−O(1)	2.369(5) (×8)	2.151(1) (×2)	1.903(2) (×2)	2.3163(1) (×2)
U−O(2)		2.142(2) (×2)	2.191(1) (×4)	2.013(4) (×4)
U−O(3)		2.151(2) (×2)		
O(1)−U−O(1)	70.5(1)	180	180	180
O(2)−U−O(2)		180	180	180
O(3)−U−O(3)		180		
O(1)−U−O(2)		91.4	90	90
O(1)−U−O(3)		91.6		
O(2)−U−O(3)		89.1		

bond length or angle (Å or deg)	γ-UO_3[31]		bond length or angle (Å or deg)	$UO_2(NO_3)_2{\cdot}6H_2O$[32]
U−O(1)	1.887(5) (×2)	2.344(6) (×2)	U−O(1)	1.770(7) (×1)
U−O(2)	2.230(3) (×4)	2.274(5) (×2)	U−O(1′)	1.749(7) (×1)
U−O(3)		1.796(6) (×2)	U−O(2)	2.504(5) (×2)
U−O(3)		3.045(6) (×2)	U−O(3)	2.547(6) (×2)
O(1)−U−O(1)	180	71.2	U−O(4)	2.397(3) (×2)
O(2)−U−O(2)	180	130.8	O(1)−U−O(1′)	179.1
O(3)−U−O(3)		174.6		
O(1)−U−O(2)	88.8	79.0		
O(1)−U−O(3)		133.0		
O(2)−U−O(3)		91.1		

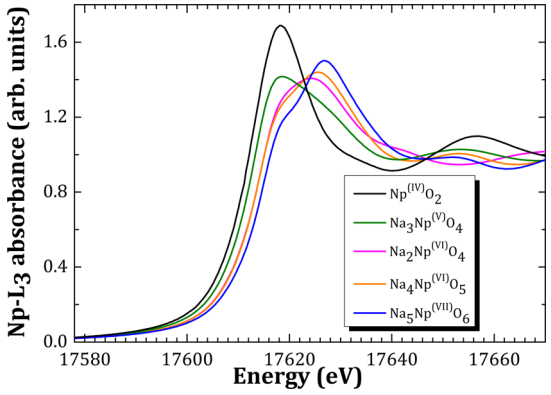

Figure 4. XANES spectra collected at the Np-L_3 edge.

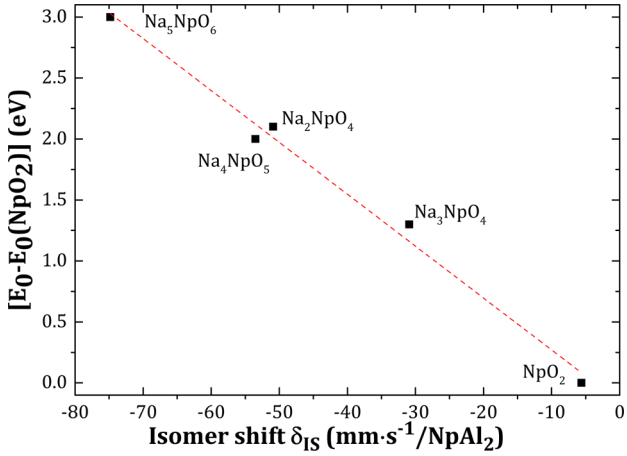

Figure 6. Absorption edge threshold E_0 relative to NpO_2 versus isomer shift measured by Mössbauer spectroscopy.

that of α-Na_2UO_4. Na_4NpO_5 has the "reverse" neptunyl configuration, with two long axial bonds at 2.31(1) Å and

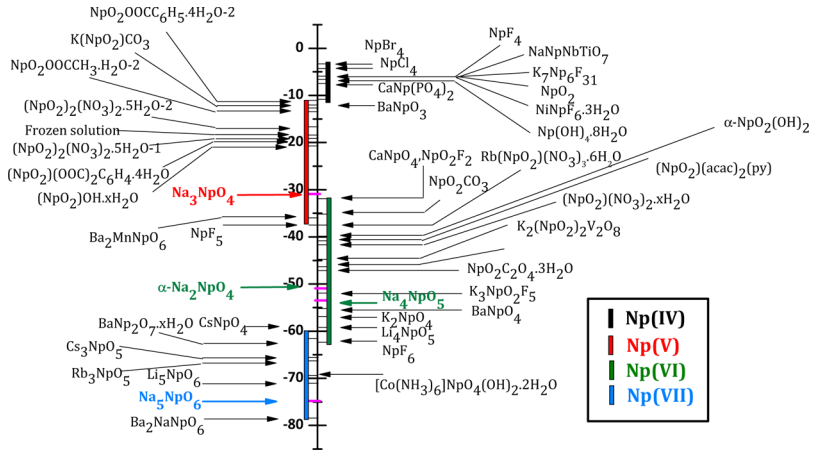

Figure 5. Isomer shifts versus $NpAl_2$ of Np(IV), Np(V), Np(VI), and Np(VII) compounds[47] together with Na_3NpO_4 (red),[26] α-Na_2NpO_4,[45] Na_4NpO_5[30] (green), and Na_5NpO_6 (blue).[30]

DOI: 10.1021/acs.inorgchem.5b02476
Inorg. Chem. 2016, 55, 1569−1579

Table 7. Local Geometry, Bond Lengths, and Bond Angles around the Neptunium Cation in NpO_2, α-Na_3NpO_4, α-Na_2NpO_4, Na_4NpO_5, and Na_5NpO_6

bond length or angle (Å or deg)	NpO_2[44]	α-Na_3NpO_4[26]	α-Na_2NpO_4[6]	Na_4NpO_5[30]	Na_5NpO_6[30]
Np−O(1)	2.353(5) (×8)	2.417(6) (×2)	1.762(5) (×2)	2.31(1) (×2)	2.08(1) (×2)
Np−O(2)		2.300(6) (×2)	2.086(5) (×4)	2.05(1) (×4)	2.07(1) (×4)
Np−O(3)		2.066(6) (×2)			
O(1)−Np−O(1)	70.5(1)	87.0(1)	180	180	180
O(2)−Np−O(2)		93.0(1)	180	180	180
O(3)−Np−O(3)		179.0(3)			
O(1)−Np−O(2)		177.0(1)	90	90	85.8(1)
O(1)−Np−O(3)		89.6(2)			
O(2)−Np−O(3)		90.4(1)			

Table 8. Local Geometry, Bond Lengths and Bond Angles around the Plutonium Cation in PuO_2, Na_4PuO_5, and Na_5PuO_6

bond length or angle (Å or deg)	PuO_2[44]	Na_4PuO_5[9]	Na_5PuO_6[19]
Pu−O(1)	2.336(5) (×8)	2.31(1) (×x2)	2.09(1) (×2)
Pu−O(2)		2.03(1) (×4)	2.03(1) (×4)
O(1)−Pu−O(1)	70.5(1)	180	180
O(2)−Pu−O(2)		180	180
O(1)−Pu−O(2)		90	87.0(1)

four short equatorial bonds at 2.05(1) Å. In this case, a low-energy shoulder is observed instead of the secondary shoulder mentioned for the uranium analogue. The latter could result from the unoccupied 6d states of the neptunium having the $[Rn]5f^1$ electronic configuration. Finally, the NpO_6 octahedra of $Na_5Np^{(VII)}O_6$ are distorted with an axial O(1)−Np-O(1) bond tilted by 85.8(1)° with respect to the equatorial plane (Figure 7). The two WLs are well separated for this compound with $[Rn]5f^0$ electronic configuration. Their relative intensities (the second WL being the most intense) are identical to that reported for the $NpO_4(OH)_2^{3-}$ complex[48,49] formed in strongly alkaline solution.

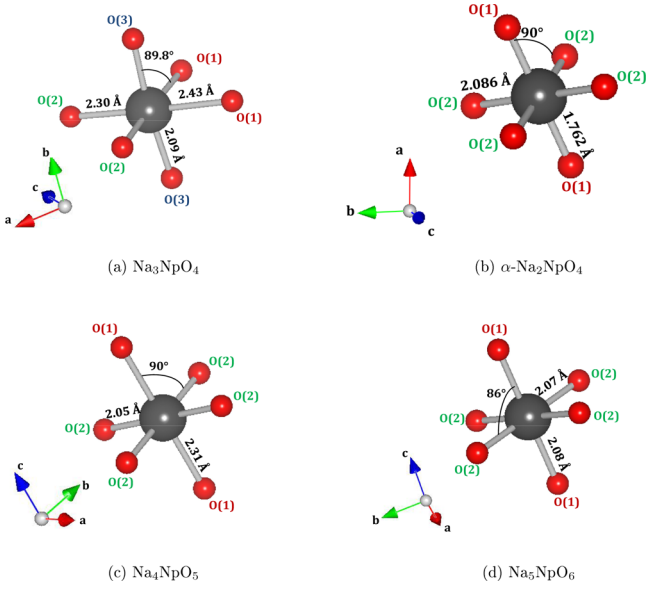

Figure 7. Sketch of the NpO_6 octahedra in (a) Na_3NpO_4, (b) α-Na_2NpO_4, (c) Na_4NpO_5, and (d) Na_5NpO_6.

XANES Spectroscopy of Sodium Plutonates. The XANES spectra of the sodium plutonates collected at the Pu-L_3 edge are shown in Figure 8 together with the spectrum of

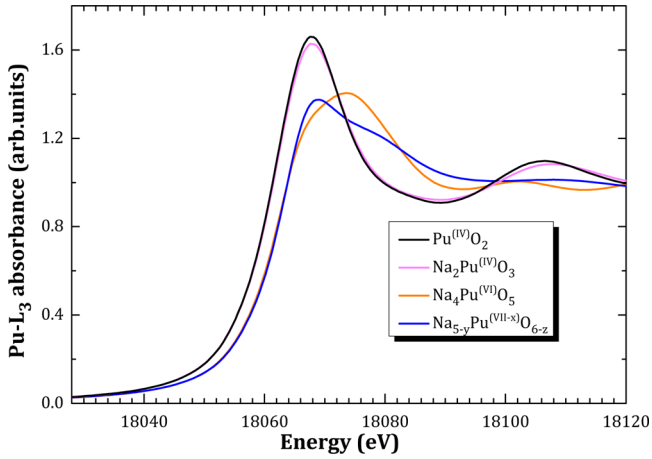

Figure 8. XANES spectra collected at the Pu-L_3 edge.

the $Pu^{(IV)}O_2$ reference material.[50,51] The energy positions of the inflection points and of the white lines are provided in Table 5. Conradson et al.[51] reported an extensive review of XANES results obtained at the Pu-L_3 edge for Pu(0)−Pu(VII) phases both in solution and as solids covering a multitude of bonding environments (chalcogenides, chlorides, hydrates, hydroxides, nitrates, carbonates, oxo−hydroxides, etc.). The authors looked in particular at the effects of ligand polarizibility, local disorder, and medium in addition to the usual correlations in terms of valence and site symmetry[51] on the energy and shape of the XANES spectra and showed the interpretation was manifold and rather complex.

The inflection point and white line values of Na_2PuO_3 are very close to those of $Pu^{(IV)}O_2$, indicating a pure Pu(IV) valence state. As for Na_4PuO_5 and Na_5PuO_6, isostructural with Na_4NpO_5 and Na_5NpO_6, they correspond to pure Pu(VI) and Pu(VII) valence states, respectively. An increase in the edge absorption energy is observed with increasing formal Pu valence state in the same manner as for the uranium and neptunium phases (Table 5), and a shoulder is observed after the main absorption peak for Pu(VI) and Pu(VII) compounds. The edge absorption energies of Pu(IV) and Pu(VI) sodium plutonate phases are found slightly lower than for the solid carbonate complexes $Pu^{(IV)}(CO_3)_5^{6-}$ and $Pu^{(VI)}O_2(CO_3)_3^{4-}$ as reported by Conradson et al.[51] This comparison illustrates the effect on the edge energies of the ligand polarizability and its correlation with bond lengths,[51] suggested the following

DOI: 10.1021/acs.inorgchem.5b02476
Inorg. Chem. 2016, 55, 1569−1579

spectroscopic series for the ability to lower the edge energy: actinyl oxo > S^{2-} > Te^{2-} > Se^{2-} > B^{3-} > Cl^{-} > O^{2-} > OH^{-} > OSiO > CO_3^{2-} > NO_3^{-} > H_2O, in good agreement with the present experimental observations. The difference obtained herein in the edge absorption energy between Pu(IV) and Pu(VI), i.e., 0.8 eV, is also smaller than for the solid carbonate complexes (1.4 eV). The local symmetries are the same as for the uranium and neptunium structural analogues: Na_4PuO_5 shows the reverse plutonyl configuration with bonds at 2.03(1) and 2.31(1) Å. The PuO_6 octahedra are distorted in the case of Na_5PuO_6, with an axial bond forming an angle of 87.0(1) Å with respect to the equatorial plane. The shape of the XANES spectrum of Na_4PuO_5 is similar to that Na_4NpO_5. The relative intensities of the first and second WLs in Na_5NpO_6 and Na_5PuO_6 (noted $Na_{5-y}PuO_{6-z}$ in Figure 8) are inverted, while the features appear slightly less resolved for the plutonium phase. The latter inversion is rather surprising as the relative intensities of Np(VII) and Pu(VII) were found identical for the complexes formed in alkaline solution.[49,52] One could therefore question the valence stability of Na_5PuO_6 under the X-ray beam, especially since the edge absorption energy of Pu(VII) (18063.5(5) eV) is found very close to that of Pu(VI) (18062.9(5) eV). No change was noticed, however, during the successive acquisitions of XANES spectra. Alternatively, the sample might have absorbed water during transport to the beamline and decomposed to Pu(VI). Complementary studies are needed to clarify this point.

XANES Systematics along the Series U−Np−Pu. The present results have shown that the correlations usually established between the shape of the XANES spectra, local coordination environment, and associated multiple scattering resonance could be more intricate. In particular, the shoulder and reduced peak amplitude found about 15 eV above the edge absorption threshold do not seem to be an exclusive characteristic of the actinyl compounds.

It is also instructive to compare the edge absorption thresholds E_0 measured for the sodium actinide oxide series relative to the edge absorption thresholds for the tetravalent actinide dioxides $E_0(MO_2)$ (M = U, Np, Pu). The neptunium series shows a linear variation of $E_0 - E_0(MO_2)$ versus the formal valence state of the actinide cation, but this is not true for the uranium compounds (Figure 9). The latter feature could be related to the degree of "localization" of the 5f electrons and to the difference between the formal valence states assigned by XANES and XRD and the real charge distributions. However, electronic density calculations would be required to substantiate such interpretation.

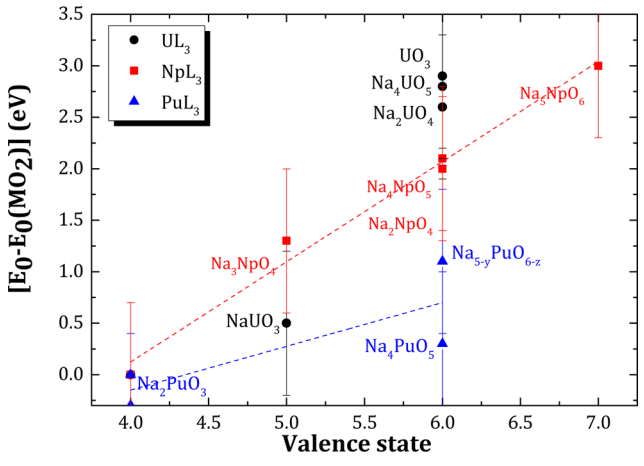

Figure 9. Absorption edge threshold E_0 relative to MO_2 (M = U, Np, Pu) versus valence state for the sodium actinide ternary oxides.

The energy needed to excite an electron from the 2p core-hole to the 5f/6d electronic states diminishes along the series U−Np−Pu as clearly illustrated by the isostructural compounds Na_2UO_4/Na_2NpO_4 and $Na_4UO_5/Na_4NpO_5/Na_4PuO_5$. This behavior is expected in relation with the decreasing size of the cationic radii (or number of 5f electrons) and specific bonding characteristics of the 5f shells. The 5f electrons from thorium to neptunium show an "itinerant" or "delocalized" character, meaning they are available for covalent bonding.[53] By contrast, the 5f electrons from americium to lawrencium are more "localized". Plutonium stands at the limit between the two behaviors and shows localized or delocalized characteristics depending on conditions of pressure, temperature, and magnetic field.[53] For a given oxidation state, the more localized the 5f electrons are (toward Pu) and the more numerous the 5f shells are, the greater is the Coulomb energy and hence the easier it is to eject an electron from the 2p core−shell.

CONCLUSIONS

A Rietveld refinement of monoclinic Na_2PuO_3, in space group $C2/c$, has been reported for the first time in this work, and the existence of Na_2NpO_3 has been revealed. In addition, XANES spectra of Np(IV), Np(V), Np(VI), Np(VII), Pu(IV), Pu(VI), and Pu(VII) sodium actinide ternary oxide phases have been collected in the solid state. The sodium actinate series provide a variety of local coordination geometries around the 6-fold-coordinated actinide cation (actinyl, reverse actinyl, distorted octahedra). The present studies have shown that the XANES features usually attributed to multiple scattering resonance of the actinyl compounds could also be found for other types of geometry. This observation suggests that the mechanisms in the solid state are probably more intricate and that other factors could be at play for the latter geometries. The double-peak WL features of the An(V), An(VI), and An(VII) compounds (An = U, Np, Pu) could possibly originate from core-ionized final states with different 5f occupancies, as already pointed out in the literature on the basis of high-pressure XANES experiments at the U-L_3 edge. We can also suggest possible effects of the degree of localization of the 5f electrons. Electronic density calculations would be required to provide more insight into the underlying mechanisms.

Finally, the reported data can serve as a reference for mixed oxide compounds with sodium, i.e., sodium urano−plutonates and sodium urano−neptunates, which are of particular relevance for understanding the interaction chemistry between the nuclear fuel $(U,Np,Pu)O_2$ and the sodium coolant in sodium-cooled fast reactors. Indeed, the information on the valence state can be used to assess the oxygen potential threshold required within the fuel and sodium coolant for the formation of these sodium actinide ternary oxides and therefore to estimate the margin to the safe operation of SFRs.

ASSOCIATED CONTENT

Supporting Information

The Supporting Information is available free of charge on the ACS Publications website at DOI: 10.1021/acs.inorgchem.5b02476.

X-ray diffraction patterns for the studied materials (ZIP)

DOI: 10.1021/acs.inorgchem.5b02476
Inorg. Chem. 2016, 55, 1569−1579

First- and second-differential XANES data for all compounds (PDF)

X-ray crystallographic file of Na_2PuO_3 in CIF format (CIF)

AUTHOR INFORMATION

Corresponding Authors

*E-mail: a.l.smith@tudelft.nl.

*E-mail: rudy.konings@ec.europa.eu.

Present Address

§A.L.S.: Delft University of Technology, Radiation Science & Technology Department, Nuclear Energy and Radiation Applications (NERA), Mekelweg 15, 2629 JB Delft, The Netherlands.

Notes

The authors declare no competing financial interest.

ACKNOWLEDGMENTS

The authors would like to thank Dr. G. Peter-Soldani and Dr. E. Welcomme for kindly providing us their XANES data on the uranyl nitrate hexahydrate $UO_2(NO_3)_2{\cdot}6H_2O$. The authors acknowledge the 7th Framework Program of the European Commission and the Joint Advanced Severe Accidents Modeling and Integration for Na-cooled neutron reactors (JASMIN) programme (reference 295803). XAS experiments at the ESRF have been supported by the European FP7 TALISMAN project, under contract with the European Commission. The authors thank TALISMAN and the ESRF for provision of beamtime. A.L.S. acknowledges the European Commission and the Ras al Khaimah Centre for Advanced Materials for funding her Ph.D. studentship.

REFERENCES

(1) *Annual report 2013*; GIF (Generation IV International Forum): 2013. https://www.gen-4.org/gif/jcms/c_64097/2013-gif-annual-report.

(2) *Technology Roadmap Update for Generation IV Nuclear Energy Systems*; GIF (Generation IV International Forum): 2014. https://www.gen-4.org/gif/upload/docs/application/pdf/2014-03/gif-tru2014.pdf.

(3) Koch, L. *J. Less-Common Met.* **1986**, *122*, 371−382.

(4) Walker, C. T.; Nicolaou, G. *J. Nucl. Mater.* **1995**, *218*, 129−138.

(5) Smith, A. L.; Raison, P. E.; Martel, L.; Charpentier, T.; Farnan, I.; Prieur, D.; Hennig, C.; Scheinost, A.; Konings, R. J. M.; Cheetham, A. K. *Inorg. Chem.* **2014**, *53*, 375−382.

(6) Smith, A. L.; Raison, P. E.; Konings, R. J. M. *J. Nucl. Mater.* **2011**, *413*, 114−121.

(7) Pillon, S. Etude des diagrammes de phases U-O-Na, Pu-O-Na et U,Pu-O-Na. Ph.D. Thesis, Université Du Languedoc, 1989.

(8) Pillon, S.; Ingold, F.; Fischer, P.; Andre, G.; Botta, F.; Stratton, R. W. *J. Nucl. Mater.* **1993**, *206*, 50−56.

(9) Bykov, D.; Raison, P.; Konings, R. J. M.; Apostolidis, C.; Orlova, M. *J. Nucl. Mater.* **2015**, *457*, 54−62.

(10) Guerin, Y. In *Comprehensive Nuclear Materials*; Konings, R. J. M., Allen, T. R., Stoller, R. E., Yamanaka, S., Eds.; Elsevier, 2012; Vol. 2, Chapter 2.21: Fuel Performance of Fast Spectrum Oxide Fuel, pp 547−578.

(11) Mignanelli, M. A.; Potter, P. E. *J. Nucl. Mater.* **1983**, *114*, 168−180.

(12) Mignanelli, M. A.; Potter, P. E. *J. Nucl. Mater.* **1984**, *125*, 182−201.

(13) Mignanelli, M. A.; Potter, P. E. *J. Nucl. Mater.* **1985**, *130*, 289−297.

(14) Blackburn, P. E.; Hubbard, W. K. Proceedings of Conference on Fast Reactor Fuel Element Technology; Hinsdale, Illinois, 1972; p 479.

(15) Housseau, M.; Dean, G.; Perret, F. *Behaviour and Chemical State of Irradiated Ceramic Fuels*. Panel Proceedings Series. IAEA: Vienna, 1974; p 349.

(16) Housseau, M.; Dean, G.; Marcon, J.-P.; Marin, J. F. Report CEA-N-1588 (Commissariat á l'énergie atomique et aux énergies alternatives)., 1973.

(17) Adamson, M. G.; Mignanelli, M. A.; Potter, P. E.; Rand, M. H. *J. Nucl. Mater.* **1981**, *97*, 203−212.

(18) Mignanelli, M. A.; Potter, P. E. *Thermochim. Acta* **1988**, *129*, 143−160.

(19) Smith, A. L. Structural and Thermodynamic Properties of Sodium Actinide Ternary Oxides. Ph.D. Thesis, University of Cambridge, 2015.

(20) Rossberg, A.; Scheinost, A. C.; Schmeisser, N.; Rothe, J.; Kaden, P.; Schild, D.; Wiss, T.; Daehn, R. AcReDaS, an Actinide Reference Database for XAS, EELS, IR, Raman and NMR Spectroscopy; https://www.hzdr.de/acredas, 2014.

(21) Unger, L. M.; Trubey, D. K. *Specific Gamma-Ray Dose Constants for Nuclides Important to Dosimetry and Radiological Assessment. ORNL/RSIC-45/RI*; 1982.

(22) Rodriguez-Carvajal, J. *Phys. B* **1993**, *192*, 55−69.

(23) Matz, W.; et al. *J. Synchrotron Radiat.* **1999**, *6*, 1076−1085.

(24) Ravel, B.; Newville, M. *J. Synchrotron Radiat.* **2005**, *12*, 537−541.

(25) Van den Berghe, S.; Leenaers, A.; Ritter, C. *J. Solid State Chem.* **2004**, *177*, 2231−2236.

(26) Smith, A. L.; Raison, P. E.; Hen, A.; Bykov, D.; Colineau, E.; Sanchez, J.-P.; Konings, R. J. M.; Cheetham, A. K. *Dalton Transactions* **2015**, *44*, 18370−18377.

(27) Smith, A. L.; Raison, P. E.; Martel, L.; Prieur, D.; Charpentier, T.; Wallez, G.; Suard, E.; Scheinost, A. C.; Hennig, C.; Martin, P.; Kvashnina, K. O.; Cheetham, A. K.; Konings, R. J. M. *Inorg. Chem.* **2015**, *54*, 3552−3561.

(28) Cordfunke, E. H. P.; IJdo, D. J. W. *J. Solid State Chem.* **1995**, *115*, 299−304.

(29) Roof, I. P.; Smith, M. D.; zur Loye, H.-C. *J. Cryst. Growth* **2010**, *312*, 1240−1243.

(30) Smith, A. L.; Hen, A.; Raison, P. E.; Colineau, E.; Griveau, J.-C.; Magnani, N.; Sanchez, J. P.; Konings, R. J. M.; Caciuffo, R.; Cheetham, A. K. *Inorg. Chem.* **2015**, *54*, 4556−4564.

(31) Loopstra, B. O.; Taylor, J. C.; Waugh, A. B. *J. Solid State Chem.* **1977**, *20*, 9−19.

(32) Taylor, J. C.; Mueller, M. H. *Acta Crystallogr.* **1965**, *19*, 536−543.

(33) Doi, Y.; Ninomiya, K.; Hinatsu, Y.; Ohoyama, K. *J. Phys.: Condens. Matter* **2005**, *17*, 4393−4401.

(34) Hinatsu, Y.; Doi, Y. *J. Alloys Compd.* **2006**, *418*, 155−160.

(35) Mogare, K. M.; Friese, K.; Klein, W.; Jansen, M. *Z. Anorg. Allg. Chem.* **2004**, *630*, 547−552.

(36) Shannon, R. D. *Acta Crystallogr., Sect. A: Cryst. Phys., Diffr., Theor. Gen. Crystallogr.* **1976**, *32*, 751−767.

(37) Le Bail, A. *Powder Diffr.* **2005**, *20*, 316−326.

(38) Panin, R. V.; Khasanova, N. R.; Abakumov, A. M.; Antipov, E. V.; Van Tendeloo, G.; Schnelle, W. *J. Solid State Chem.* **2007**, *180*, 1566−1571.

(39) Urland, W.; Hoppe, R. *Z. Anorg. Allg. Chem.* **1972**, *392*, 23−36.

(40) Bertram, S.; Kaindl, G.; Jové, J.; Pagès, M.; Gal, J. *Phys. Rev. Lett.* **1989**, *63*, 2680−2683.

(41) Bertram, S.; Kaindl, G.; Jové, J.; Pagès, M. *Phys. B* **1989**, *158*, 508−510.

(42) Antonio, M.; Soderholm, L. In *The Chemistry of the Actinide and Transactinide Elements*; Morss, L. R., Edelstein, N., Fuger, J., Katz, J. J., Eds.; Springer: Dordrecht, The Netherlands, 2006; Chapter 28: X-ray absorption spectroscopy of the actinides, pp 3086−3198.

DOI: 10.1021/acs.inorgchem.5b02476
Inorg. Chem. 2016, 55, 1569−1579

(43) Soldatov, A. V.; Lamoen, D.; Konstantinovic, M. J.; Van den Berghe, S.; Scheinost, A. C.; Verwerft, M. *J. Solid State Chem.* **2007**, *180*, 54−61.
(44) Yamashita, T.; Nitani, N.; Tsuji, T.; Inagaki, H. *J. Nucl. Mater.* **1997**, *245*, 72−78.
(45) Smith, A. L.; Hen, A.; Raison, P. E.; Colineau, E.; Griveau, J.-C.; Magnani, N.; Sanchez, J. P.; Konings, R. J. M.; Caciuffo, R.; Cheetham, A. K. *J. Phys.: Condens. Matter* **2016**, *28*, 086002.
(46) Dickson, D. P. E.; Berry, F. J. *Mössbauer spectroscopy*; Cambridge University Press: New York, 2005.
(47) Yoshida, Z.; Johnson, S. G.; Kimura, T.; Krsul, J. R. In *The Chemistry of the Actinide and Transactinide Elements*; Morss, L. R., Edelstein, N., Fuger, J., Katz, J. J., Eds.; Springer: Dordrecht, The Netherlands, 2006; Chapter 6: Neptunium, pp 699−812.
(48) Williams, C. W.; Blaudeau, J.-P.; Sullivan, J. C.; Antonio, M. R.; Bursten, B.; Soderholm, L. *J. Am. Chem. Soc.* **2001**, *123*, 4346−4347.
(49) Bolvin, H.; Wahlgren, U.; Moll, H.; Reich, T.; Geipel, G.; Fanghänel, T.; Grenthe, I. *J. Phys. Chem. A* **2001**, *105*, 11441−11445.
(50) Martin, P.; Grandjean, S.; Ripert, M.; Freyss, M.; Blanc, P.; Petit, T. *J. Nucl. Mater.* **2003**, *320*, 138−141.
(51) Conradson, S. D.; et al. *Inorg. Chem.* **2004**, *43*, 116−131.
(52) Antonio, M. R.; Williams, C. W.; Sullivan, J. A.; Skanthakumar, S.; Hu, Y.-J.; Soderholm, L. *Inorg. Chem.* **2012**, *51*, 5274−5281.
(53) Konings, R. J. M.; Benes, O.; Griveau, J.-C. *Comprehensive Nuclear Materials*; Konings, R. J. M., Allen, T. R., Stoller, R. E., Yamanaka, S., Eds.; Elsevier, 2012; Vol. 2, Chapter 2.01: The Actinides Elements: Properties and Characteristics, pp 1−20.

DOI: 10.1021/acs.inorgchem.5b02476
Inorg. Chem. 2016, 55, 1569−1579